IEEE Access
Multidisciplinary | Rapid Review | Open Access Journal

Received April 13, 2020, accepted April 21, 2020, date of publication April 27, 2020, date of current version May 13, 2020.

Digital Object Identifier 10.1109/ACCESS.2020.2990634

A BPSO-Based Method for Optimal Voltage Sag Monitor Placement Considering Uncertainties of Transition Resistance

HAIWEI JIANG, YONGHAI XU, (Member, IEEE), ZITENG LIU, NING MA, AND WENQING LU, (Graduate Student Member, IEEE)

State Key Laboratory of Alternate Electrical Power System with Renewable Energy Sources, North China Electric Power University, Beijing 102206, China

Corresponding author: Yonghai Xu (yonghaixu@263.net)

This work was supported by the National Natural Science Foundation of China under Grant 51277069.

ABSTRACT This study presents a new approach to the optimal placement of voltage sag monitors considering the uncertainties associated with transition resistance. The influence of transition resistance on the magnitude of voltage sags triggered by symmetrical and unsymmetrical faults is analyzed. Then the transition resistance interval set array for voltage sags is established, on the basis of which, a random vector model on voltage sag observability is proposed and related observability indices are defined in the form of conditional probability. The optimal placement model is established by taking the available number of monitors as the constraint condition and the maximum sag global observability index as the objective function. Binary particle swarm optimization (BPSO) is implemented to obtain the optimal placement results. Finally, simulation is carried out on IEEE 30-bus system, and it is shown that the proposed optimal monitor placement method is more applicable compared with the traditional MRA method.

INDEX TERMS Binary particle swarm optimization, conditional probability, observability indices, optimal monitor placement, random vector model, transition resistance, uncertainties, voltage sags.

I. INTRODUCTION

Voltage sags are the most frequently occurring power quality disturbances, mainly caused by faults in a power system. Voltage sag is typically defined as the reduction of RMS voltage from 0.1 to 0.9 p.u. with a typical duration of 0.5 cycle to 1 min, which is usually characterized by its magnitude (the magnitude of during-fault voltages) and duration (the time during which the RMS voltage stays below a given threshold, usually 0.9 p.u.) [1]–[4].

Many studies conducted around the world have shown that voltage sags cause customers of various sectors significant financial losses, for instance, in a semiconductor manufacturing industry, economic losses per voltage sag have been estimated 3.8 million €[5], [6]. But it is unrealistic to expect that the grid will provide a completely financial-loss-free power quality environment for all customers [6]. Before implementing adequate countermeasures, it is necessary to establish a monitoring system by using appropriate power quality monitors (PQMs) and this system should enable each voltage sag in the considered network to be detected [6]–[8].

As a means of obtaining voltage sag data and assessing voltage sag performance, power quality monitoring is a stated consensus that it will play a key role in the advancement of power systems infrastructure [6]. The ideal voltage sag monitoring system consists of PQMs installed at all buses in the considered network [7], [8]. However, it is unrealistic for economic reasons. And it is showed that the reduction of the number of PQMs will be conductive to decreasing the cost of the monitoring system and the quantity of data recorded by PQMs [9]. Therefore, with the permission of economic condition, how to develop methods to assess the number and the strategic locations of monitors to detect more voltage sags is still required. Fortunately, in recent years, several studies have been attempted to solve the PQM placement problem by determining the optimal number and locations of PQMs.

Since voltage sags are mostly caused by symmetrical and unsymmetrical faults, the main idea of monitoring voltage sags is to make any fault-initiated voltage sag event observed at least by one monitor. The first and foremost approach

The associate editor coordinating the review of this manuscript and approving it for publication was Hui Ma.

to optimal voltage sag monitor placement is monitor reach area (MRA) method, in which the minimum number of monitors can be required to capture the voltage sags generated by three phase metallic short circuits at all buses by integer linear programming [9]. The MRA method is further extended for unsymmetrical short circuits in order to record more different characteristics of voltage sags [10]. To make the optimal placement program more precise, a method expressed in [11] deals with uncovered line faults, which are ignored by the original MRA method. Besides, in order to find the result of optimal replacement in a short time, a method of simultaneously analyzing different types of faults is proposed by obtaining a reduced observability matrix [12]. Moreover, a variety of optimization methods, including Genetic Algorithm, Binary Particle Swarm Optimization (BPSO) and etc. are presented to find the minimum number of PQMs and their best arrangement [7], [9], [13]–[15].

However, transition resistance, which is of stochastic nature, frequently exists at the fault positions when short-circuit faults occur [16], [17]. As the uncertainties of transition resistance is not considered in the MRA method, the expected observability of the optimal placement program is not guaranteed in the practical field of engineering. A fault location method is attempted to weaken the defects derived from the transition resistance [6]. But there may be some issues in fault location-based methods for voltage sag monitoring, when the impedance model of network is inaccurate or when several points are found as a fault location [17]. Furthermore, according to the definition of the voltage sags, the short-circuit faults are not equivalent to voltage sags [1]–[5]. Replacing the target of monitoring voltage sag with the fault location may lead to a large number of monitoring devices being installed [12], [18].

In this paper, taking the uncertainties of transition resistance as well as the common statistics and aggregation principle of monitoring into sufficient consideration, a novel optimal voltage sag monitor placement method based on probability theory and BPSO is proposed. The main contribution of this work is threefold:

1) We classify the voltage sag magnitudes for different fault types, regarding voltage sag magnitudes as functions of the transition resistance values, and analyze the impact transition resistance has on voltage sag magnitudes in detail.
2) We establish a three-dimensional random vector model with the transition resistance along with fault position and fault type viewed as random variables. Besides, we define two observability indices from the perspective of conditional probability, which could effectively analyze the voltage sag observability for monitoring system.
3) Based on the proposed model, we propose a new optimal monitor placement method, which could determine the optimal placement results in presence of transition resistance uncertainties for any number of provided PQMs. And the optimization problem is solved by using BPSO algorithm, in which the condition of swarm position updating is modified accordingly.

This paper is organized as follows. Section II formulates the analytical expressions of residual phase voltage caused by non-metallic faults. Section III briefly recalls the traditional optimal monitoring method and demonstrates its shortcoming. Section IV analyses the impact transition resistance has on voltage sag magnitudes. In section V, a random vector model is established to analyze voltage sag observability for monitoring system. The proposed optimal monitoring placement model and its solving method are presented in Section VI. In section VII, the proposed method is implemented and tested on the IEEE 30-bus test system. Finally, the conclusions are presented in Section VIII.

II. CALCULATION OF REMAINING VOLTAGES

Since voltage sags are mostly caused by short-circuit faults, this paper focuses on the fault-initiated voltage sags [1]–[10]. In this section, the residual phase voltage (during-fault voltage) equations for four types of faults are formulated, which are the basic prerequisites of subsequent analyses.

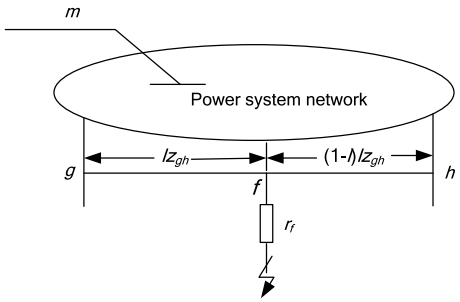

FIGURE 1. Short-circuit fault calculation model of power system.

As is shown in Fig.1, m is the monitoring position, f is fault position at the line connecting buses g and h, r_f is transition resistance, and l is the distance between fault position f and bus g, which can be expressed as

$$l = \frac{L_{gf}}{L_{gh}} \tag{1}$$

where L_{gf} is the distance between fault position f and bus g. L_{gh} is the total length of line g-h.

The sequence mutual impedances corresponding to bus m and fault position f as well as the sequence self impedances of fault position f can be expressed as follows

$$Z^u_{mf} = (1-l)Z^u_{mg} + lZ^u_{mh} \tag{2}$$

$$Z^u_{ff} = (1-l)^2 Z^u_{gg} + l^2 Z^u_{hh} + 2l(1-l)Z^u_{gh} + l(1-l)z^u_{gh} \tag{3}$$

where u represents the sequence of impedance such that its value is taken as 1, 2, and 0 for positive, negative,

and zero sequence of impedance, respectively. Z^u_{mg} are the sequence mutual impedances corresponding to buses m and g. Z^u_{mh} are the sequence mutual impedances corresponding to buses m and h. Z^u_{gh} are the sequence mutual impedances corresponding to buses g and h. Z^u_{gg} and Z^u_{hh} represent the sequence self impedances at buses g and h. z^u_{mg} are the sequence line impedances between buses g and h.

According to the superposition theorem, the residual phase voltage is the sum of the prefault voltage and the fault component. Hence, considering that the prefault voltage of each bus is 1p.u., when short-circuit faults of different types occur at any point along a general line connecting buses g and h, the residual phase voltages at bus m can be expressed by the prefault voltages and the sequence impedances, using the method of symmetrical components [19]–[22].

A. THREE-PHASE FAULT (3PF)

Only positive sequence should be considered for the balanced fault and the residual voltage at bus m for a three-phase fault can be expressed as [22]

$$\dot{U}_{m,A,B,C} = 1 - \frac{Z^1_{mf}}{Z^1_{ff} + r_f} \tag{4}$$

B. SINGLE LINE-TO-GROUND FAULT (SLGF)

When a SLGF occurs at phase A, the residual phase voltages at bus m can be expressed as [22]

$$\begin{cases} \dot{U}_{m,A} = 1 - \dfrac{Z^0_{mf} + Z^1_{mf} + Z^2_{mf}}{Z^0_{ff} + Z^1_{ff} + Z^2_{ff} + 3r_f} \\ \dot{U}_{m,B} = a^2 - \dfrac{Z^0_{mf} + a^2 Z^1_{mf} + a Z^2_{mf}}{Z^0_{ff} + Z^1_{ff} + Z^2_{ff} + 3r_f} \\ \dot{U}_{m,C} = a - \dfrac{Z^0_{mf} + a Z^1_{mf} + a^2 Z^2_{mf}}{Z^0_{ff} + Z^1_{ff} + Z^2_{ff} + 3r_f} \end{cases} \tag{5}$$

where a is the complex number operator, e^{j120°.

C. LINE-TO-LINE FAULT (LLF)

Positive and negative sequences are considered for LLF. When a LLF occurs between phase B and C, the residual phase voltages at bus m can be expressed as [22]

$$\begin{cases} \dot{U}_{m,A} = 1 - \dfrac{Z^1_{mf} - Z^2_{mf}}{Z^1_{ff} - Z^2_{ff} + r_f} \\ \dot{U}_{m,B} = a^2 - \dfrac{\alpha^2 Z^1_{mf} - a Z^2_{mf}}{Z^1_{ff} - Z^2_{ff} + r_f} \\ \dot{U}_{m,C} = a - \dfrac{\alpha Z^1_{mf} - a^2 Z^2_{mf}}{Z^1_{ff} - Z^2_{ff} + r_f} \end{cases} \tag{6}$$

D. DOUBLE LINE-TO-GROUND FAULT (DLGF)

When a DLGF occurs at phases B and C, the residual phase voltages at bus m can be expressed as [22]

$$\begin{cases} \dot{U}_{m,A} = 1 \\ \dfrac{Z^1_{mf}(Z^2_{ff} + Z^0_{ff} + 3r_f) - Z^2_{mf}(Z^0_{ff} + 3r_f) - Z^0_{mf} Z^2_{ff}}{Z^1_{ff}(Z^2_{ff} + Z^0_{ff} + 3r_f) + Z^2_{ff}(Z^0_{ff} + 3r_f)} \\ \dot{U}_{m,B} = a^2 \\ \dfrac{a^2 Z^1_{mf}(Z^2_{ff} + Z^0_{ff} + 3r_f) - a Z^2_{mf}(Z^0_{ff} + 3r_f) - Z^0_{mf} Z^2_{ff}}{Z^1_{ff}(Z^2_{ff} + Z^0_{ff} + 3r_f) + Z^2_{ff}(Z^0_{ff} + 3r_f)} \\ \dot{U}_{m,C} = \alpha \\ \dfrac{a Z^1_{mf}(Z^2_{ff} + Z^0_{ff} + 3r_f) - a^2 Z^2_{mf}(Z^0_{ff} + 3r_f) - Z^0_{mf} Z^2_{ff}}{Z^1_{ff}(Z^2_{ff} + Z^0_{ff} + 3r_f) + Z^2_{ff}(Z^0_{ff} + 3r_f)} \end{cases} \tag{7}$$

III. TRADITIONAL OPTIMAL MONITORING METHOD

A. OPTIMAL MONITORING METHOD BASED ON MRA

Monitor Reach Area (MRA) can be regarded as a set consisting of fault positions for a given meter position [9]. When a fault occurs at any position in this set, a PQM at the meter position will be triggered to record voltage sag as the lowest measured residual voltage magnitude of the phase voltages is lower than the given threshold (usually 0.9 p.u.). MRA is usually expressed as a binary matrix of order $(N \times F)$, where N is the number of observation buses and F is the number of fault positions. The value 1 in entry (i, j) of the matrix indicates that fault position j belongs to the MRA of a meter at bus i. Otherwise, the element of the matrix is 0. The MRA matrix is built for each type of fault and given voltage threshold U_{th}, which is expressed as

$$MRA_{t,ij} = \begin{cases} 1, & V_{t,ij} \le U_{th} \\ 0, & V_{t,ij} > U_{th} \end{cases} \quad \forall i, j \tag{8}$$

where i represents an arbitrary meter position; j represents an arbitrary fault position; t represents a given fault type. $V_{t,ij}$ is the lowest residual voltage magnitude of the phase voltages at bus i when a fault of type t takes place at the fault position, which can be obtained according to (4)-(7). The decision vector X of length N is defined to exhibit the need for a meter at bus i. Arbitrary element of X is expressed as

$$x_i = \begin{cases} 1, & \text{if monitor is needed at } i \\ 0, & \text{if monitor is not needed at } i \end{cases} \tag{9}$$

In order to ensure that every voltage sag can be recorded by at least one monitor when the short-circuit fault occurs at any position of the entire network, which means that the union of the MRA of each monitor must contain all buses and lines of the monitored system for arbitrary element in line i of MRA_t, the decision vector X should be subject to the following constraint

$$\sum_{i=1}^{N} x_i MRA_{t,ij} \ge b_j \tag{10}$$

where t is the fault type, b_j is the needed number (usually 1) of monitors that can record a voltage sag originated from a fault at position j.

Taking the minimum number of monitors as the objective and (10) as the constraint, the optimal number and arrangement can be determined by solving a 0-1 integer linear programming problem.

B. THE SHORTCOMINGS OF MRA MODEL

Among most MRA-based methods, the transition resistance is ignored, which means that the value of r_f in (4)-(7) is assumed as zero when calculating the remaining voltage [6]–[15]. However, transition resistance actually exists for short-circuit faults, whose value is of a stochastic nature under the impact of short-circuit medium type, phase-to-phase distance, earth conductivity and other factors [16], [23]–[25]. As a result, when a short-circuit fault occurs at a fault position, the relationship between $V_{t,ij}$ and U_{th} in size is also random. As is shown in (8), since the value of each element in the MRA matrix is exactly determined by the fixed relationship between the $V_{t,ij}$ and U_{th}, it is difficult for the MRA matrix to objectively describe the region of the network where the monitor is able to register voltage sags.

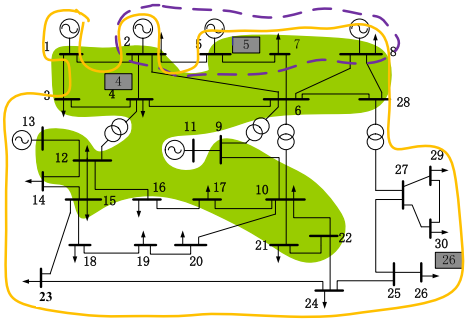

FIGURE 2. The MRA for metallic SLGF ($r_f = 0\Omega$).

In order to explain the shortcomings resulting from transition resistance being ignored, the MRA-based method with a voltage threshold of 0.9 p.u. is applied to optimal monitor placement in the IEEE30-bus system in the section. The result shows that three monitors installed at buses 4, 5 and 26 are sufficient to cover the entire network on condition that the value of transition resistance is zero. In practice, however, the MRA is greatly affected by the transition resistance. For instance, the MRA of the three monitors due to SLGF with r_f equal to 0Ω and 5Ω are shown in Fig.2 and Fig.3 respectively, in which the area 1 (marked in green), 2 (marked in blue) and 3 (marked in yellow) are the MRA of the PQM at bus 4, 5 and 26 respectively. As we can see, compared with the case where r_f is 0Ω, the full observability of the network can be no longer achieved by the monitors when r_f is equal to 5Ω, as a large number of monitoring blind areas are shown in Fig.3. It means that once the fault occurs in the monitoring blind areas with r_f equal to 5Ω, the sags may still occur at the buses near the fault position, but neither monitors will

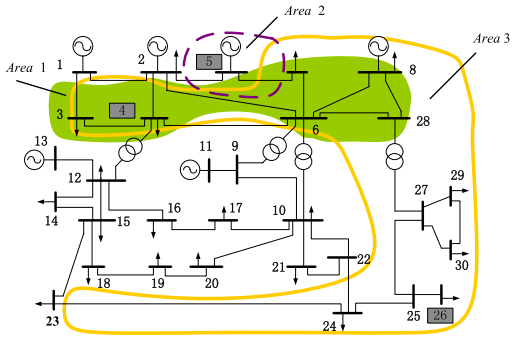

FIGURE 3. The MRA for non-metallic SLGF ($r_f = 5\Omega$).

be triggered. For example, when non-metallic SLGF with transition resistance of 5Ω occurs at bus 19, according to the voltage sag magnitude obtained by short-circuit calculation, voltage sags occur at the buses 15, 18, 19, 20 and 23. But since the fault position is located in the monitoring blind area, the three monitors at the selected meter position lost the ability to detect the voltage sags at these five buses.

Thus, from the above analysis, since the impacts transition resistance has on the MRAs are not considered, the observability of voltage sags can't be reflected objectively by the MRA-based optimization model, resulting in the prevalence of monitoring blind areas. Therefore, in this study, the uncertainties associated with transition resistance is taken into full consideration to overcome the aforementioned shortcomings of the traditional optimal sag monitoring programme.

IV. ANALYSIS OF TRANSITION RESISTANCE IMPACT ON VOLTAGE SAG MAGNITUDE

As can be seen from the analysis in the previous section, the change of transition resistance has a great impact on the range of the monitor's MRA because of the impact transition resistance has on the voltage sag magnitude. In this section, voltage sag magnitudes for different fault types are classified and the laws of voltage sag magnitudes of each type varying with the transition resistance values are mathematically analyzed in detail.

A. CLASSIFICATION OF VOLTAGE SAG MAGNITUDES

Viewed as functions of the transition resistance values, the voltage sag magnitudes for different fault types can be divided into two types according to the function forms, where the sag magnitudes for 3PF, SLGF and LLF can be classified into the same type and the sag magnitude for DLGF belongs to the other type individually.

1) VOLTAGE SAG MAGNITUDE OF TYPE-I

According to (4)-(6), the remaining phase voltages associated with 3PF, SLGF and LLF can be uniformly expressed as

$$\dot{U}_{m,p} = O \cdot \left(1 - \frac{1}{\alpha_1 \cdot r_f + \alpha_2}\right) \tag{11}$$

where p represents fault phase, O represents complex number operator, and parameters α_1 and α_2 are the complex numbers related to sequence impedance Z^u_{mf} and Z^u_{ff}, respectively. Since the lowest residual voltage magnitude only occurs in the fault phase, merely the fault phase is considered in the following research. The parameters O, α_1 and α_2 corresponding to the three types of faults are given in Table 1.

TABLE 1. Expressions of O, $\alpha 1$ and $\alpha 2$.

Fault type	Fault phase	O	α_1	α_2
3PF	A/B/C	1	$\frac{Z^1_{ff}}{Z^1_{mf}}$	$\frac{1}{Z^1_{mf}}$
SLGF	A	1	$\frac{Z^0_{ff}+Z^1_{ff}+Z^2_{ff}}{Z^0_{mf}+Z^1_{mf}+Z^2_{mf}}$	$\frac{3}{Z^0_{mf}+Z^1_{mf}+Z^2_{mf}}$
LLF	B	a^2	$\frac{Z^1_{ff}-Z^2_{ff}}{Z^1_{mf}-Z^2_{mf}/a}$	$\frac{1}{1/\left(Z^1_{mf}-Z^2_{mf}/a\right)}$
LLF	C	a	$\frac{Z^1_{ff}-Z^2_{ff}}{Z^1_{mf}-aZ^2_{mf}}$	$\frac{1}{1/(Z^1_{mf}-aZ^2_{mf})}$

By (11) and Table 1, the expression of phase magnitude for sags caused by 3PF, SLGF and LLF can be given in the same form as (12), which is called "voltage sag magnitude of type-I" in this paper.

$$\begin{cases} U^I_{m,p}=\sqrt{1-\dfrac{a_{11}r_f+b_{11}}{a_{12}r_f^2+b_{12}r_f+c_{11}}}<1, \quad r_f\in[0,+\infty) \\ a_{11}=2R_{12} \\ b_{11}=2R_{11}-1 \\ a_{12}=R_{12}^2+X_{12}^2 \\ b_{12}=2R_{11}R_{12}+2X_{11}X_{12} \\ c_{11}=R_{11}^2+X_{11}^2 \end{cases} \tag{12}$$

where R_{11} and R_{12} are the real parts of α_1 and α_2 respectively; X_{11} and X_{12} are the imaginary parts of α_1 and α_2 respectively. Additionally, according to the domain and range of $U^I_{m,p}$, it can be known that the constant terms except b_{12} in (12) are all positive-real numbers in any conditions.

2) VOLTAGE SAG MAGNITUDE OF TYPE-II

According to (7), the remaining phase voltages associated with DLGF can be uniformly expressed as

$$\dot{U}_{m,p}=O\cdot\left(1-\frac{\beta_1\cdot r_f+\beta_2}{\beta_3\cdot r_f+\beta_4}\right) \tag{13}$$

where β_1, β_2, β_3 and β_4 are also the parameters related to the sequence impedance Z^u_{mf} and Z^u_{ff}, and the meanings of p and O are the same with those of (11). Similarly, the parameters O, β_1, β_2, β_3 and β_4 are given in Table 2 with the fault phase(s) only considered.

By (13) and Table 2, the expression of phase magnitude for sags caused by DLGF can be given as (14), which is called

TABLE 2. Expressions of O, β_1, β_2, β_3 and β_4.

	Phase A	*Phase* B
O	a^2	a
β_1	$3\left(Z^1_{mf}-Z^2_{mf}/a\right)$	$3\left(Z^1_{mf}-aZ^2_{mf}\right)$
β_2	$Z^0_{mf}Z^1_{ff}-Z^0_{mf}Z^2_{ff}/a^2$ $-Z^0_{mf}Z^2_{ff}/a+Z^1_{mf}Z^2_{ff}$	$Z^0_{mf}Z^1_{ff}-Z^0_{mf}Z^2_{ff}/a$ $-aZ^0_{mf}Z^2_{ff}+Z^1_{mf}Z^2_{ff}$
β_3	$3\left(Z^1_{mf}+Z^2_{mf}\right)$	$3\left(Z^1_{mf}+Z^2_{mf}\right)$
β_4	$Z^0_{ff}Z^1_{ff}+Z^0_{ff}Z^2_{ff}+Z^1_{ff}Z^2_{ff}$	$Z^0_{ff}Z^1_{ff}+Z^0_{ff}Z^2_{ff}+Z^1_{ff}Z^2_{ff}$

"voltage sag magnitude of type- II" in this paper.

$$\begin{cases} U^{II}_{m,p}=\sqrt{\dfrac{a_{21}r_f^2+b_{21}r_f+c_{21}}{a_{22}r_f^2+b_{22}r_f+c_{22}}}<1, \quad r_f\in[0,+\infty) \\ a_{21}=(R_{23}-R_{21})^2+(X_{23}-X_{21})^2 \\ b_{21}=2\left[(R_{23}-R_{21})(R_{24}-R_{22})\right. \\ \quad \left.+(X_{23}-X_{21})(X_{24}-X_{22})\right] \\ c_{21}=(R_{24}-R_{22})^2+(X_{24}-X_{22})^2 \\ a_{22}=R_{23}^2+X_{23}^2 \\ b_{22}=2(R_{23}R_{24}+X_{23}X_{24}) \\ c_{22}=R_{24}^2+X_{24}^2 \end{cases} \tag{14}$$

where R_{21}, R_{22}, R_{23} and R_{24} are the real parts of β_1, β_2, β_3 and β_4 respectively; X_{21}, X_{22}, X_{23} and X_{24} are the imaginary parts of β_1, β_2, β_3 and β_4 respectively.

B. TRANSITION RESISTANCE IMPACT ON VOLTAGE SAG MAGNITUDE

Although the voltage sag magnitude functions of transition resistance can be divided into only two types in (12) and (14), the variation law of voltage sag magnitude for each type with transition resistance is not unique.

1) TRANSITION RESISTANCE IMPACT ON SAG MAGNITUDE OF TYPE-I

The derivative function of $U^I_{m,p}$ in (12) can be expressed as follows

$$\begin{cases} (U^I_{m,p})'=\dfrac{p\left(\lambda_1 r_f^2+\lambda_2 r_f+\lambda_3\right)}{\left(a_{12}r_f^2+b_{12}r_f+c_{11}\right)^2} \\ p=\dfrac{1}{2}\left(1-\dfrac{a_{11}r_f+b_{11}}{a_{12}r_f^2+b_{12}r_f+c_{11}}\right)^{\frac{-1}{2}} \\ \lambda_1=a_{11}a_{12}; \quad \lambda_2=2a_{12}b_{11}; \ \lambda_3=b_{11}b_{12}-a_{11}c_{11} \end{cases} \tag{15}$$

Whether $(U^I_{m,p})'$ is positive or negative depends on the distribution of the quadratic function $(\lambda_1 r_f^2+\lambda_2 r_f+\lambda_3)$ within the domain $r_f\in[0,+\infty)$. Since λ_1 and λ_2 are always positive numbers, as shown in Fig.4, the monotonicity of $U^I_{m,p}$ can

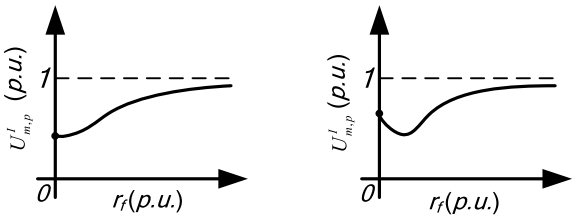

(a) Type A_1 (b) Type B_1

FIGURE 4. The relationship curve between $U^{I}_{m,p}$ and r_f ($U^{I}_{m,p} - r_f$ curve).

TABLE 3. Monotonic types of $U^{I}_{m,p}$ on different conditions.

Monotonicity condition	*Monotonicity type*
$\lambda_3 \le 0$	Type A_1
$\lambda_3 > 0$	Type B_1

be divided into two types merely according to the different values of λ_3 in Table 3. Besides, it can be noted that $U^{I}_{m,p}$ would approach 1p.u. with r_f close to infinity.

2) TRANSITION RESISTANCE IMPACT ON SAG MAGNITUDE OF TYPE-II

The derivative function of $U^{II}_{m,p}$ in (14) can be expressed as follows

$$\begin{cases} (U^{II}_{m,p})' = p_2 \dfrac{\gamma_1 r_f^2 + \gamma_2 r_f + \gamma_3}{\left(a_{22} r_f^2 + b_{22} r_f + c_{22}\right)^2} \\ p_2 = \dfrac{1}{2}\left(\dfrac{a_{21} r_f^2 + b_{21} r_f + c_{21}}{a_{22} r_f^2 + b_{22} r_f + c_{22}}\right)^{\frac{-1}{2}} \\ \gamma_1 = a_{21} b_{22} - a_{22} b_{21} \\ \gamma_2 = 2\,(a_{21} c_{22} - a_{22} c_{21}) \\ \gamma_3 = b_{21} c_{22} - b_{22} c_{21} \end{cases} \tag{16}$$

Similarly, whether $(U^{II}_{m,p})'$ is positive or negative also depends on the distribution of a quadratic function $(\gamma_1 r_f^2 + \gamma_2 r_f + \gamma_3)$ within the domain $r_f \in [0, +\infty)$. However, whether the three coefficients γ_1, γ_2 and γ_3 are positive or negative is uncertain, the monotonicity of $U^{II}_{m,p}$ in (12) is more multiple than that of $U^{I}_{m,p}$ in (14). As shown in Fig.5, the monotonicity of $U^{II}_{m,p}$ can be divided into six types according to the different values of γ_1, γ_2 and γ_3 in Table 4. And it should be noted that with r_f close to infinity, $U^{II}_{m,p}$ would approach $U^{II}_{m,p}(\infty) = \sqrt{a_{21}/a_{22}}$, which is smaller than 1p.u.

V. VOLTAGE SAG OBSERVABILITY FOR MONITORING SYSTEM

A. TRANSITION RESISTANCE INTERVAL SET ARRAY

Considering the relationships between voltage sag magnitudes and transition resistance illustrated in Fig.3. and Fig.4, it can be seen that for a certain fault event, whether the

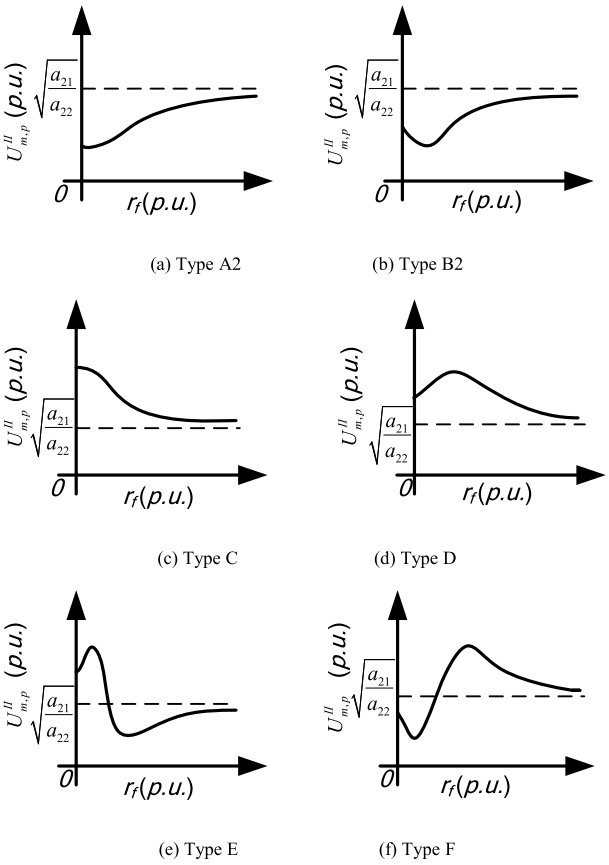

(a) Type A2 (b) Type B2

(c) Type C (d) Type D

(e) Type E (f) Type F

FIGURE 5. The relationship curve between $U^{II}_{m,p}$ and rf ($U^{II}_{m,p} - r_f$ curve).

TABLE 4. Monotonic types of $U^{II}_{m,p}$ on different conditions.

Monotonicity condition	*Monotonicity type*	*Monotonicity condition*	*Monotonicity type*
$\begin{cases}\gamma_1,\gamma_3>0\\ \gamma_2^2-4\gamma_1\gamma_3<0\end{cases}$	Type A_2	$\begin{cases}\gamma_1<0\\ \gamma_3>0\end{cases}$	Type D
$\begin{cases}\gamma_1>0\\ \gamma_3<0\end{cases}$	Type B_2	$\begin{cases}\gamma_1,\gamma_3>0\\ \gamma_2^2-4\gamma_1\gamma_3>0\end{cases}$	Type E
$\begin{cases}\gamma_1,\gamma_3<0\\ \gamma_2^2-4\gamma_1\gamma_3<0\end{cases}$	Type C	$\begin{cases}\gamma_1,\gamma_3<0\\ \gamma_2^2-4\gamma_1\gamma_3>0\end{cases}$	Type F

residual phase voltage magnitude at a bus could fall below given threshold depends on whether the value of transition resistance could fall in a distinctive interval set. In order to obtain the transition resistance interval set for each bus and each fault position, an array of phase transition resistance interval sets (PTRIS) as (17) is constructed for considered type of fault.

$$S^{t}_{p} = s^{t}_{p,ij} \quad \forall i, j. \tag{17}$$

where t represents fault type and p represents fault phase. The dimension of this array is N by F, where N is the number of buses and F is the number of fault positions. The $s^{t}_{p,ij}$ in entry (i, j) of the array represents an interval set. Only if a fault of type t takes place at the fault position j, where the value

of transition resistance falls into $s^t_{p,ij}$, can the voltage sag magnitude of phase p at bus i be below given threshold U_{th}.

In order to determine $s^t_{p,ij}$, the critical transition resistance value r_c for given voltage threshold U_{th} should be obtained by solving residual phase voltage magnitude equation for variable r_f as

$$U_{ij,p}(r_f) - U_{th} = 0 \tag{18}$$

where $U_{ij,p}(r_f)$ represents voltage sag magnitude of phase p at bus i when a fault occurs at position j.

It is important to note that according to (12) and (14), the (18) can be transformed into a quadratic equation, so the analytical solution(s) r_c for $r_c \geq 0$ can be obtained easily only by using the quadratic formula. Then, if the quadratic equation has no solution, $s^t_{p,ij}$ can be determined according to the relationship between the given threshold U_{th} and any value of $U_{ij,p}(r_f)$ for $r_f \geq 0$, whereas if the equation has solution(s), $s^t_{p,ij}$ could be determined according to the number of the solution(s) and the derivative of the solution(s). The specific methods of determining $s^t_{p,ij}$ are shown in Table 5, where N_{root} denotes the number of the solution(s) of (18).

TABLE 5. Determination Method of $s^t_{p,ij}$.

Type	N_{root}	$U_{ij,p}$ or $U_{ij,p}'$	$s^t_{p,ij}$
I	0	$\forall r_f, U_{ij,p} > U_{th}$	$\varnothing$
II	0	$\forall r_f, U_{ij,p} < U_{th}$	$[0,\infty)$
III	1	$U_{ij,p}'(r_c) > 0$	$[0,r_c)$
VI	1	$U_{ij,p}'(r_c) < 0$	(r_c,∞)
V	2	$U'_{ij,p}(r_{c,1}) < 0, U'_{ij,p}(r_{c,2}) > 0$	(r_{c1},r_{c2})
VI	2	$U'_{ij,p}(r_{c,1}) > 0, U'_{ij,p}(r_{c,2}) < 0$	$[0,r_{c1}),(r_{c2},\infty)$

It is worthwhile re-emphasizing that only the sag magnitude of fault phase(s) could exhibit the greatest deviation from nominal voltage, which contributes more to the voltage sag monitoring than that of non-faulted phase(s). So only PTRIS array for phase A, S^t_A is needed when 3PF or SLGF is considered. Similarly, only PTRIS arrays for phase A and B, S^t_B and S^t_C are needed when LLF or DLGF is considered. Then, based on S^t_A, S^t_B or S^t_C, an array of bus transition resistance interval set (BTRIS), S^t_{bus} is defined as (19) for considered type of fault, the dimension of which is the same as PTRIS array. The element $s^t_{bus,ij}$ also indicates an interval set of transition resistance. When a fault of type t occurs at position j, where the value of transition resistance falls into $s^t_{bus,ij}$, the lowest voltage sag magnitude of three phases at bus i can be lower than given threshold, in other words, the monitor installed at bus i can be triggered. Hence, the S^t_{bus} can be expressed as follows

$$S^t_{bus} = s^t_{bus,ij} = \begin{cases} s^t_{A,ij}, & t = 1,2 \\ s^t_{B,ij} \cup s^t_{C,ij}, & t = 3,4, \end{cases} \quad \forall i,j. \tag{19}$$

where t represents fault type and the value of t is 1, 2, 3, and 4 for 3PF, SLGF, LLF, and DLGF, respectively.

B. VOLTAGE SAG OBSERVABILITY RANDOM VECTOR MODEL

Evaluating the voltage sag observability of monitoring system reasonably is the key to the establishment of optimal placement model [7]–[10]. The MRA-based method achieves full observability of voltage sags by ensuring that every fault event is recorded by at least one monitor. But there is an issue that the MRA-based method takes the fault events as the observation target instead of voltage sags as the target [9]. The reason why this method is feasible is that the MRA is established only by considering the occurrence of three-phase metallic faults at each bus, which is bound to result in voltage sags at least at the faulted bus. Consequently, the observation of faults is equivalent to that of voltage sags in this scenario.

However, considering the uncertainties of transition resistance, the value of transition resistance at fault position may fall into such a range that no voltage sag occurs at any bus, which means that there are a large number of fault events that cannot belong to the observation objects of monitoring system. Thus, the fault events must be clearly classified from the perspective of monitoring voltage sags, thereafter, the studied events should be limited to the events that can cause voltage sags to achieve a reasonable evaluation of the voltage sag observability.

In order to describe the stochastic uncertainty that the voltage sags are recorded by the monitoring system in presence of transition resistance, based on the aforementioned discussion about the observation objects of monitoring system, a three-dimensional discrete random vector (Y_1, Y_2, Y_3) is introduced to characterize fault events, where Y_1 is a random variable related to the value of transition resistance, which can be indicated as

$$Y_1 = \begin{cases} 1, & \text{at least one monitor is triggered} \\ 2, & \text{no monitor is triggered but voltage sag occurs} \\ 3, & \text{no voltage sag occurs.} \end{cases} \tag{20}$$

where $\{Y_1 = 1\}$ means that at least one monitor is triggered to record voltage sag(s). $\{Y_1 = 2\}$ means that a fault causes voltage sag(s), but no monitors can record the voltage sag(s). $\{Y_1 = 3\}$ means that the fault occurs but the fault does not cause voltage sag(s), which are such event that does not belong to the observation objects of monitoring system.

The value of random variable Y_2 is fetched from 1 to F (F is the number of fault positions), representing where the fault occurs. Hence, Y_2 can be expressed as

$$Y_2 = \begin{cases} 1, & \text{when fault occurs at position 1} \\ 2, & \text{when fault occurs at position 2} \\ \cdots & \\ F, & \text{when fault occurs at position F} \end{cases} \tag{21}$$

The value of random variable Y_3 is fetched from 1 to 4, representing fault types, so Y_3 can be expressed as

$$Y_3 = \begin{cases} 1, & \text{when 3PF occurs} \\ 2, & \text{when SLGF occurs} \\ 3, & \text{when LLF occurs} \\ 4, & \text{when DLGF occurs} \end{cases} \quad (22)$$

Among the probabilities related to (Y_1, Y_2, Y_3) are the conditional probabilities, $P(Y_1 \leq 1|Y_2 = j, Y_3 = t)$ denoted by $p^t_{ps,j}$ and $P(Y_1 = 1|Y_2 = j, Y_3 = t)$ denoted by $p^t_{ms,j}$, which contribute to the subsequent analyses of voltage sag observability. The formulations of these two probabilities are presented as follows:

a. Conditional probability $p^t_{ps,j}$: $p^t_{ps,j}$ represents the probability of the occurrence of voltage sags in the power system on condition that a fault of type t occurs at position j, that is, the conditional probability of $\{Y_1 \leq 2\}$ given by $\{Y_2 = j, Y_3 = t\}$. Thus, $p^t_{ps,j}$ is just the probability of the event that transition resistance falls into the union set of the column j elements in S^t_{bus}, shown as

$$s^t_{ps,j} = \bigcup_{i=1}^{N} S^t_{bus,ij} \quad (23)$$

At this moment, the conditional probability $p^t_{ps,j}$ can be written as

$$p^t_{ps,j} = P(Y_1 \leq 2|Y_2 = j, Y_3 = t) = \sum_{k=1}^{M_{1,j}} \int_{r_{2k-1}}^{r_{2k}} f(r_f)dr \quad (24)$$

where $M_{1,j}$ represents the number of intervals contained in $s^t_{ps,j}$, and r_{2k-1} and r_{2k} represent the left and right endpoints of the k-th interval in $s^t_{ps,j}$, respectively. $f(r_f)$ is the probability density function of transition resistance.

b. Conditional probability $p^t_{ms,j}$: $p^t_{ms,j}$ represents the probability of the event that at least one monitor in a considered monitoring system is triggered on condition that a fault of type t occurs at position j, that is, the conditional probability of $\{Y_1 = 1\}$ given by $\{Y_2 = j, Y_3 = t\}$. In order to obtain the corresponding transition resistance interval set for $p^t_{ms,j}$, an array, S^t_{mon} can be constructed as (25) which is jointly formed by S^t_{bus} and the decision vector X in (9).

$$S^t_{mon} = s^t_{mon,ij} = \begin{cases} s^t_{bus,ij}, & x_i = 1 \\ \emptyset, & x_i = 0 \end{cases} \quad \forall i, j. \quad (25)$$

where $x_i = 1$ represents that a monitor is needed at bus i while $x_i = 0$ represents that no monitor is needed at bus i.

Thereafter, the transition resistance interval set related to $p^t_{ms,j}$ can be expressed as the union set of the column j elements in S^t_{mon}, which is as follows

$$s^t_{ms,j} = \bigcup_{i=1}^{N} s^t_{mon,ij} \quad (26)$$

Consequently, the conditional probability $p^t_{ms,j}$ can be written as

$$p^t_{ms,j} = P(Y_1 = 1|Y_2 = j, Y_3 = \text{t}) = \sum_{k=1}^{M_{2,j}} \int_{r_{2k-1}}^{r_{2k}} f(r_f)dr \quad (27)$$

where $M_{2,j}$ represents the number of intervals contained in $s^t_{ms,j}$, and r_{2k-1} and r_{2k} represent the left and right endpoints of the k-th interval in $s^t_{ms,j}$, respectively.

C. VOLTAGE SAG OBSERVABILITY INDICES

Based on the proposed random vector model, two probabilistic observability indices are defined, which could effectively analyze the voltage sag observability for monitoring system.

1) VOLTAGE SAG LOCAL OBSERVABILITY INDEX

The Sag Local Observability Index (SLOI) defined in this paper refers to the probability of the event that voltage sag(s) can be recorded by monitoring system, under the condition that a fault of a ''certain'' type at a ''certain'' fault position has caused voltage sag(s), that is, the conditional probability of $\{Y_1 = 1\}$ given by $\{Y_1 \leq 2, Y_2 = j, Y_3 = t\}$. According to the condition probability equation, the SLOI associated with fault type t and fault position j can be calculated as

$$SLOI^t_j = P(Y_1 = 1|Y_1 \leq 2, Y_2 = j, Y_3 = \text{t}) = \frac{p^t_{ms,j}}{p^t_{ps,j}} \quad (28)$$

where $p^t_{ps,j}$ and $p^t_{ms,j}$ are shown in equations (24) and (27), respectively.

2) VOLTAGE SAG GLOBAL OBSERVABILITY INDEX

The Sag Global Observability Index (SGOI) defined in this paper refers to the probability of the event that voltage sag(s) can be recorded by monitoring system, under the condition that a fault of a ''random'' type at a ''random'' fault position has caused voltage sag(s), that is, the conditional probability of $\{Y_1 = 1\}$ given by $\{Y_1 \leq 2\}$. As can be seen, compared with the expression of SLOI in (28), SGOI cancels the limitation of the certainties of fault position and fault type, which indicates that not only the uncertainties of transition resistance but also that of fault positions and fault types are considered. According to the full probability equation and condition probability equation, SGOI can be expressed as

$$SGOI = P(Y_1 = 1|Y_1 \leq 2) = \frac{\sum_{t=1}^{4}\sum_{j=1}^{F} \omega_t \lambda_j p^t_{ms,j}}{\sum_{t=1}^{4}\sum_{j=1}^{F} \omega_t \lambda_j p^t_{ps,j}} \quad (29)$$

where λ_j equal to $P(Y_2 = j)$ represents the probability of a fault event at position j, and ω_t equal to $P(Y_3 = t)$ represents the probability of a type-t fault event.

Compared with equations (28) and (29), it can be seen that SGOI can be regarded as the average value of all SLOIs corresponding to each certain fault position and fault type with λ_j and ω_t as weights. Besides, it is worthwhile to note that if n_f is used to represent the total number of faults randomly occurring in the entire network over a period of time, SGOI can be also expressed as $n_f \sum_{t=1}^{4}\sum_{j=1}^{F} \lambda_j \omega_t p^t_{ms,j} / n_f \sum_{t=1}^{4}\sum_{j=1}^{F} \lambda_j \omega_t p^t_{ps,j}$, which is the ratio of the expected value of total number of

voltage sags recorded by a monitoring system to the expected value of total number of voltage sags actually occurring in the power system. Therefore, for voltage sag monitoring, the larger the achieved SGOI value, the greater the number of voltage sags recorded by monitoring system and the higher the overall level of all SLOIs.

VI. OPTIMAL VOLTAGE SAG MONITORING PROGRAMME

A. FORMULATION OF OPTIMAL SAG MONITORING PLACEMENT PROBLEM

The given optimal programme in this paper aims to provide the best arrangement of monitors, the number of which depends on investment and the cost of operation and maintenance. If the available number of monitors is n, the constraint can be described as

$$\sum [X] = n \tag{30}$$

where X is the binary decision vector shown in (9), and $\sum[X]$ represents the total number of monitors.

Under the condition that the number of available monitors is fixed, in order to achieve the maximum probability of the event that voltage sags are recorded by monitoring system, that is, to obtain a monitor arrangement with the maximum SGOI value, the objective function can be described as

$$f = \max(SGOI_X) \tag{31}$$

where $SGOI_X$ is the SGOI value corresponding to a monitoring programme whose decision vector is X.

B. OPTIMIZATION METHODS BASED ON BPSO

The defined optimization problem belongs to a discrete nonlinear programming problem with equality constraint, which should be solved by implementing meta-heuristic algorithms. Well-known meta-heuristics algorithms include Simulated Annealing, Genetic Algorithm, Ant Colony Optimization, Particle Swarm Optimization (PSO) and etc., which have all been exploited to solve the placement problem [11], [25]–[27]. Of all the population-based meta-heuristics, PSO is easy to implement, which has less dependent empirical parameters and fast convergence rate [27], [28]. But PSO is not suitable for solving discrete optimal problems. Thus BPSO, the discrete binary version of PSO, is utilized in this paper, which meets the demand that voltage sag monitors allocation can be encoded into binary forms [29].

In BPSO algorithm, a j-th bit of the i-th particle (x_{ij}) in the swarm is represented as a bit 0 or 1 in X vector (the decision vector above), which is shown in (9) whereas its movement in the space is known as velocity vector (v_{ij}) [14], [29]. Each particle updates its velocity's bits based on current velocity, the best position explored so far (P) and the global best position explored by swarm (G) as given by

$$v_{ij}(t+1) = w \cdot v_{ij}(t) + c_1\varphi_1(P_j - x_{ij}(t)) + c_2\varphi_2(G_j - x_{ij}(t)) \tag{32}$$

where w is inertia weight; c_1 and c_2 are positive acceleration coefficients; φ_1 and φ_2 are uniform random variables distributed in interval [0,1].

In the whole iterative process of the algorithm, each particle updates its position's bits, as given by

$$x_{ij}(t+1) = \begin{cases} 1, & \text{if } \rho < \dfrac{1}{1+\exp(-v_{ij}(t+1))} \\ 0, & \text{otherwise} \end{cases} \tag{33}$$

where ρ is an uniform random variable in interval [0,1].

However, in order to meet the equality constraint in (30), the following special steps of this paper are embedded in the process of applying BPSO:

a. At the beginning of the algorithm, for each particle, n (the number of available monitors) 1 should be randomly generated in its search space (particle position, X_i) so as to form a particle swarm quickly, in which all particles are within the feasible solution space.

b. When applying the update strategies of the velocity and position in (32) and (33), due to the random variable ρ in (33), it is difficult to get a swarm, in which all particles can satisfy the constraint conditions during each iteration, resulting in an endless loop. Therefore, for each particle, when the position vector X_i updated by using (33) does not meet the constraint conditions, X_i is corrected in such a way that if $\sum[X_i] > n$, n bits which are randomly selected from the current bits equal to 1 of X_i are set to 1, whereas if $\sum[X_i] < n$, (n$-\sum[X_i]$) bits which are randomly selected from the current bits equal to 0 of X_i are set to 1.

Thus, the methodology for voltage sag monitoring placement based on BPSO can be summarized in Fig.6.

VII. NUMERICAL STUDY

The proposed optimal placement method is implemented and tested on the IEEE 30-bus test system which comprises 6 sources, 30 buses, 37 transmission lines and 4 transformers with YNyn connection mode.

In this numerical study, according to [30], [31], the transition resistance follows a normal distribution with mean $\mu = 5\Omega$ and a standard deviation $\sigma = 1\Omega$. The occurrence probability of 3PF, SLGF, LLF and DLGF are assigned as $\omega_1 = 0.04$, $\omega_2 = 0.73$, $\omega_3 = 0.06$ and $\omega_4 = 0.17$, respectively [32]. Besides, when faults are simulated, each bus is considered as fault position and five fault positions with equal interval on each line are also considered, which are randomly selected from a uniform distribution. Thus, 215 fault positions are defined and probability of the occurrence of a fault at each position is assumed as $\lambda_j = 1/215$. In practical application, the fault probability of each position can be also assumed by the length of each line or determined by the fault rate of buses and lines according to historical data [33], [34]. Table 6 presents the probability corresponding to each random variable above, which are used in the subsequent simulation and analyses.

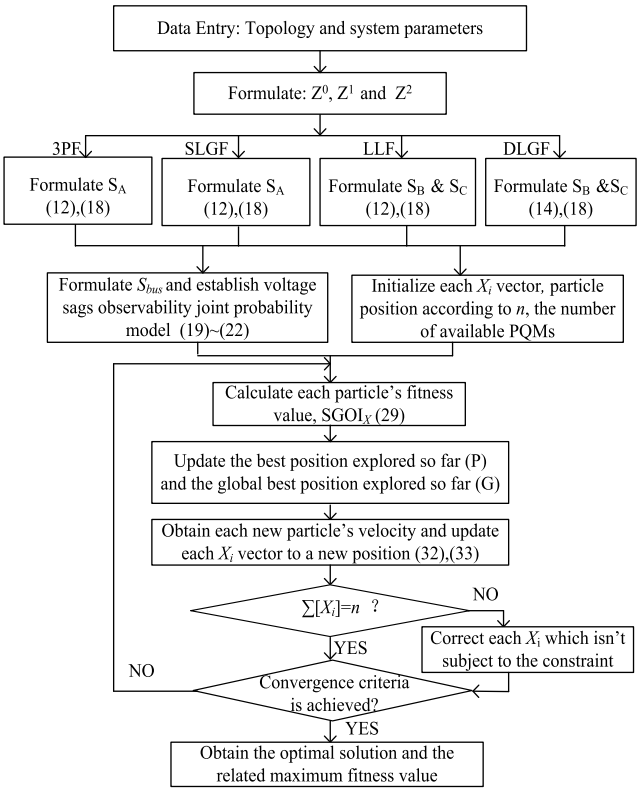

FIGURE 6. Proposed methodology flowchart based on BPSO.

A. VOLTAGE SAG OBSERVABILITY OF PLACEMENT RESULTS BASED ON MRA METHOD

It can be seen from section III that when transition resistance is ignored, the optimal placement results based on MRA method are buses 4, 5 and 26. In this subsection, the voltage sag observability of this programme for voltage threshold of 0.9 p.u. is analyzed according to the proposed voltage sag observability random vector model.

1) VOLTAGE SAG LOCAL OBSERVABILITY

The local observability index $SLOI_j^t$ of the monitoring system (buses 4, 5, and 26) related to each fault position is calculated for each fault type individually, according to (28) and Table 6. The value-frequency distribution histogram of SLOIs for each fault type is shown in Fig. 7.

TABLE 6. Parameters of random variable.

Transition resistance	*Fault type*	*Fault position*
μ=5Ω	ω_1=0.04 (3PF)	λ_j=1/215 $\forall j$
	ω_2=0.73 (SLGF)	
σ=1Ω	ω_3=0.06 (LLF)	
	ω_4=0.17 (DLGF)	

It can be seen from Fig.7 that except DLGF, the SLOIs for each type of fault are not concentrated at a high level, and the

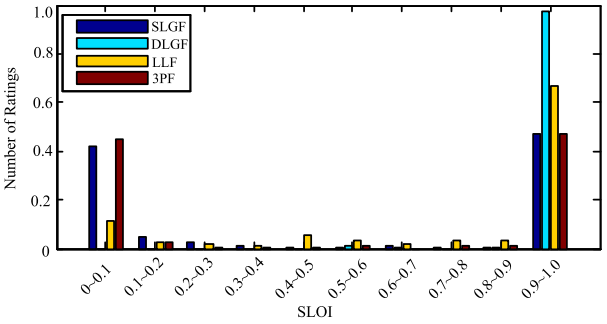

FIGURE 7. SLOI / frequency histogram corresponding to buses 4, 5 and 26.

SLOIs for 3PF and SLGF even present a U-shaped distribution, in other words, the distribution of SLOIs is polarized.

In order to more intuitively show the local observability of the monitoring system (buses 4, 5, and 26) for fault-initiated voltage sags occurring at each position, Fig.8 shows the spatial distribution of SLOIs, taking the SLGF with the highest probability as an example.

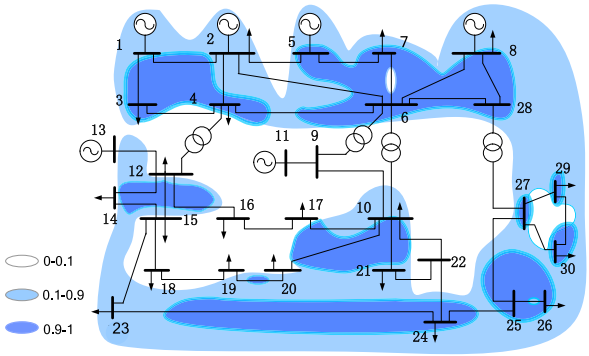

FIGURE 8. SLOI spatial distribution corresponding to buses 4, 5 and 26 for SLGF.

In Fig. 8, the regions in white, light blue and dark blue correspond to areas with SLOI of 0-0.1, 0.1-0.9 and 0.9-1, respectively. A large number of white areas in the middle of the network (covering about 42% of the simulated fault points) shows that when a single line-to-ground fault occurs at a certain position in the white area and meanwhile causes voltage sag(s) of the power system, the monitoring system can only record voltage sag(s) with a probability of less than 0.1 due to the uncertainties of the transition resistance. Thus, the unsatisfactory sag observability of MRA method emerges again.

2) VOLTAGE SAG GLOBAL OBSERVABILITY

By using (29) and Table 6, the global observability index SGOI of the monitoring system (buses 4, 5 and 26) is calculated, which is 0.6671. This SGOI value indicates that when fault-initiated voltage sag occurs, the probability of the event that the monitoring system can record the voltage sag is 0.6671, with uncertainties of transition resistance, fault positions and fault types all considered.

In order to further demonstrate the meaning of SGOI and verify the accuracy of the calculation results, Monte Carlo simulation is performed as a virtual long-term simulation to test the performance of the monitoring system, in which the characteristics of transition resistance and fault type are randomly generated according to Table 6, whereas the fault position is selected by uniform distribution from arbitrary position at all buses and lines, not only selected from the 215 positions considered above.

In the simulation, voltage-sag events occurring at multiple buses caused by the same fault are viewed as one voltage sag event for the power system. Besides, as long as the lowest residual voltage magnitude among buses 4, 5 and 26 is lower than the threshold (0.9 p.u.), it is considered that only one voltage sag event is recorded by the monitoring system. N_{sys} and N_{omp} are used to represent the current total number of sags in the power system and the total number of sags recorded by the monitoring system, respectively. 3000 faults are simulated, and the variations of N_{omp}/N_{sys} with the number of simulations are shown as Fig.9.

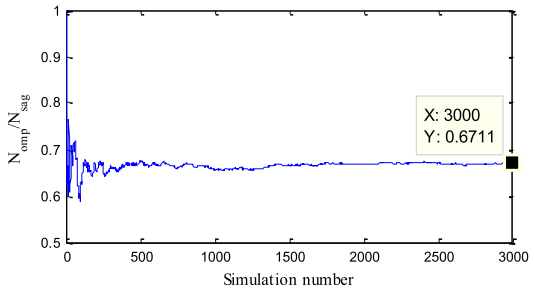

FIGURE 9. Variations of N_{omp}/N_{sys}.

It can be seen from Fig.9 that the ratio of N_{sys} to N_{omp} finally converges to a small neighborhood of 0.6711, which is almost completely consistent with the value of SGOI (0.6671) calculated in this paper. Therefore, only a single SGOI value can describe the probability of a event that a monitoring system can record voltage sag(s) when a fault of a random type at a random fault position has caused voltage sag(s).

Since the value of SGOI for MRA method is only 0.6671, merely about 66.71% of voltage sag events can be recorded for a period of time. Thus, a more satisfactory placement of monitors is needed.

B. PLACEMENT RESULTS OF THE PROPOSED METHOD

The simulation platform uses the computer with dual core CPU, whose main frequency is 3.20 GHz and the memory is 6GB. According to the process shown in Fig. 5, BPSO is implemented to explore the solution space, which is programmed in MATLAB environments. The population size is 20 and the maximum number of iterations is 200. Besides, an adaptive inertia weight is used in BPSO.

The convergence curve shows variations of the fitness value with the number of iterations. Average convergence curves for four different numbers (n = 3, 5, 7 and 9) of

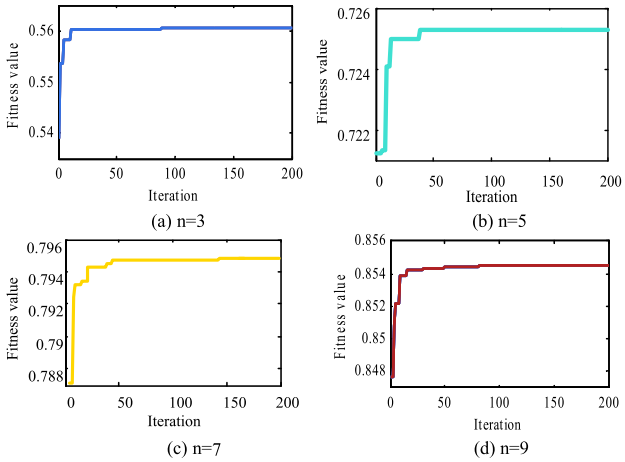

FIGURE 10. Average convergence curves.

monitors are shown in Fig. 10. It can be seen that the particle swarm converges in all the cases, which means that the method of achieving the equality constraints in section VI is feasible as the particle swarm whose positions are "corrected" can still explore the optimal solution within the feasible solution space. Additionally, each iteration only takes about 2.82 seconds, meaning that the optimal solution can be obtained in less than 10 minutes. Since the optimal configuration is offline in the engineering application, the execution time of the algorithm is completely acceptable.

Table 7 shows the optimization results and the corresponding maximum fitness value ($SGOI_{max}$) obtained by BPSO for different numbers of monitors when voltage threshold of each monitor is 0.9 p.u.

TABLE 7. Optimization results using the proposed method.

Number of monitors	Location of monitors	SGOI
1	24	0.6207
2	18, 25	0.7627
3	15, 22, 27	0.8394
4	2, 15, 21, 25	0.8821
5	2, 15, 16, 21, 25	0.9208
6	2, 5, 15, 16, 21, 25	0.9452
7	2, 5, 15, 16, 20, 21, 25	0.9616
8	1, 2, 5, 14, 16, 18, 21, 25	0.9782
9	1, 2, 5, 14, 16, 17, 18, 22, 25	0.9856
10	1, 2, 5, 14, 15, 16, 17, 20, 22, 25	0.9928

As shown in Table 7, if the resources are so limited for planners that only one monitor can be provided, bus 24 should be selected as a monitor position. At this moment, the value of SGOI is 0.6207, which is close to that of MRA method. When two monitors can be provided, buses 18 and 25 are the best choice, whose value of SGOI is 0.7627. Not only is the SGOI value of this programme higher than that of the MRA method, but also the number of needed monitors is smaller than that of the MRA method.

Whereas when the number of monitors is the same as the result of MRA method, it can be seen that the result (buses

15, 22, and 27) of the proposed method can achieve the SGOI value of 0.8394, which is 17.23% higher than that of MRA method. Additionally, for the results with the same number of monitors as the MRA method, Fig.11 presents the value-frequency distribution of SLOIs for each fault type and Fig.12 presents the spatial distribution of SLOIs for single line-to-ground fault. Compared with Fig. 7 and Fig. 8, it can be seen that SLOIs present a J-shaped distribution, which means that the distribution of SLOIs is centralized in a higher level.

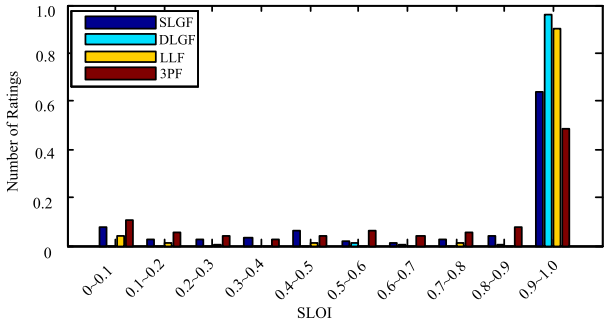

FIGURE 11. SLOI / frequency histogram corresponding to buses 15, 22 and 27.

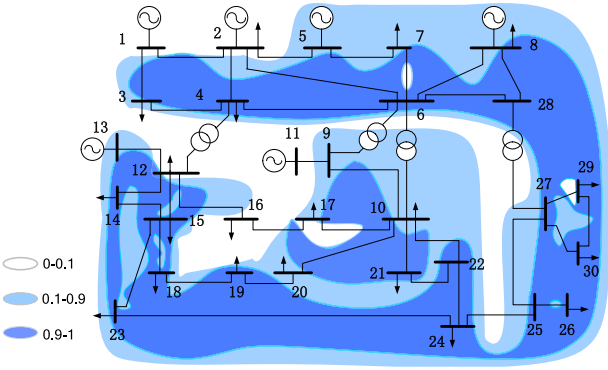

FIGURE 12. SLOI spatial distribution corresponding to buses15, 22 and 27 for SLGF.

The more monitors can be provided, the higher the maximum value of SGOI can be achieved. In practical engineering application, the appropriate placement programme can be selected by considering the installation costs and the requirements of the value of SGOI.

VIII. CONCLUSION

Transition resistance is an indispensable characteristic of short-circuit faults, which has been introduced into the optimal voltage sag monitor placement in this paper. The observability of voltage sags has probability attribute in presence of the uncertainties of transition resistance. Based on probability theory, this paper defined and quantified the observability of voltage sags in the form of conditional probability. Applying BPSO technique, the proposed method can provide the best arrangement for any number of monitors to achieve the maximum global observability of voltage sags. Several detailed conclusions are obtained:

1) When considered as the function of transition resistance at a fault position, voltage sag magnitudes can be classified into two types. The variation law of the sag magnitudes with the transition resistance is not unique. When a fault occurs, whether the sag magnitude can be lower than given threshold depends on whether the value of transition resistance can fall into a corresponding interval set.
2) Since not all faults could initiate voltage sag(s), the observability of voltage sags defined in this paper aims to describe the probability of the event that monitoring system can record voltage sag(s) under the condition that a fault has caused voltage sag(s). Based on the appropriate formation of PTRIS and BTRIS arrays, the voltage sag observability random vector model is proposed and the observability of voltage sags is described as two indices (SLOI and SGOI) in the form of conditional probability. SLOI is established for certain position and type of fault (i.e. only the uncertainties of transition resistance considered) while SGOI is established for the uncertainties of not only transition resistance but also the type and position of faults.
3) The proposed novel optimal placement methodology can determine the best monitor arrangement for any number of monitors with the maximum SGOI value. BPSO is used to solve the formulated optimal problem and the equality constraint is realized by correcting the particle position at each iteration. Simulations performed on the IEEE30-bus system and the results showed that the proposed placement method achieves more satisfactory performance considering the uncertainties of transition resistance, compared with the traditional method.

REFERENCES

[1] M. H. Bollen, *Understanding Power Quality Problems*. New York, NY, USA: IEEE Press, 2000.

[2] J. R. Camarillo-Penaranda and G. Ramos, "Characterization of voltage sags due to faults in radial systems using three-phase voltage ellipse parameters," *IEEE Trans. Ind. Appl.*, vol. 54, no. 3, pp. 2032–2040, May 2018.

[3] *IEEE Draft Recommended Practice for Monitoring Electric Power Quality*, Standard P1159/D6, Jan. 2019, pp. 1–104.

[4] Y. Han, Y. Feng, P. Yang, L. Xu, Y. Xu, and F. Blaabjerg, "Cause, classification of voltage sag, and voltage sag emulators and applications: A comprehensive overview," *IEEE Access*, vol. 8, pp. 1922–1934, 2020.

[5] A. B. Baggini, *Handbook of Power Quality*. Hoboken, NJ, USA: Wiley, 2008.

[6] M. Avendano-Mora and J. V. Milanovic, "Monitor placement for reliable estimation of voltage sags in power networks," *IEEE Trans. Power Del.*, vol. 27, no. 2, pp. 936–944, Apr. 2012.

[7] R. Alicic and S. Smaka, "A new approach to optimal placement of power quality monitors for voltage sag detection," in *Proc. IEEE PES Innov. Smart Grid Technol. Eur. (ISGT-Europe)*, Sep. 2019, pp. 1–5.

[8] M. A. Eldery, E. F. El-Saadany, M. M. A. Salama, and A. Vannelli, "A novel power quality monitoring allocation algorithm," *IEEE Trans. Power Del.*, vol. 21, no. 2, pp. 768–777, Apr. 2006.

[9] G. Olguin, F. Vuinovich, and M. H. J. Bollen, "An optimal monitoring program for obtaining voltage sag system indexes," *IEEE Trans. Power Syst.*, vol. 21, no. 1, pp. 378–384, Feb. 2006.
[10] E. Espinosa-Juarez, A. Hernandez, and G. Olguin, "An approach based on analytical expressions for optimal location of voltage sags monitors," *IEEE Trans. Power Del.*, vol. 24, no. 4, pp. 2034–2042, Oct. 2009.
[11] C. F. M. Almeida and N. Kagan, "Allocation of power quality monitors by genetic algorithms and fuzzy sets theory," in *Proc. Int. Intell. Syst. Appl. Power Syst.*, São Paulo, Brazil, Nov. 2009, pp. 1–6.
[12] T. R. Kempner, M. Oleskovicz, and D. P. S. Gomes, "Optimal monitoring of voltage sags through simultaneous analysis of short-circuits in distribution systems," *IET Gener., Transmiss. Distrib.*, vol. 11, no. 7, pp. 1801–1808, May 2017.
[13] A. A. Ibrahim, A. Mohamed, H. Shareef, and S. P. Ghoshal, "Optimal power quality monitor placement in power systems based on particle swarm optimization and artificial immune system," in *Proc. 3rd Conf. Data Mining Optim. (DMO)*, Jun. 2011, pp. 141–145.
[14] A. A. Ibrahim, A. Mohamed, H. Shareef, and S. P. Ghoshal, "An effective power quality monitor placement method utilizing quantum-inspired particle swarm optimization," in *Proc. Int. Conf. Electr. Eng. Informat.*, Jul. 2011, pp. 1–6.
[15] A. A. Ibrahim, A. Mohamed, H. Shareef, and S. P. Ghoshal, "Optimization methods for optimal power quality monitor placement in power systems: A performance comparison," *Int. J. Electr. Eng. Informat.*, vol. 4, no. 1, pp. 78–91, Mar. 2012.
[16] H. Zhang and R. Che, "Fault cause identification based on characteristics of transition resistances for transmission lines," in *Proc. 5th Int. Conf. Electr. Utility Deregulation Restructuring Power Technol. (DRPT)*, Nov. 2015, pp. 1405–1409.
[17] S. Nasiri and H. Seifi, "Robust probabilistic optimal voltage sag monitoring in presence of uncertainties," *IET Gener., Transmiss. Distrib.*, vol. 10, no. 16, pp. 4240–4248, Dec. 2016.
[18] M. Avendano-Mora, N. C. Woolley, and J. V. Milanovic, "On improvement of accuracy of optimal voltage sag monitoring programmes," in *Proc. 14th Int. Conf. Harmon. Qual. Power - ICHQP*, Sep. 2010, pp. 1–6.
[19] P. M. Anderson. *Analysis of Faulted Power Systems*. Ames, IA, USA: Iowa State Univ. Press, 1973.
[20] N. Wu, J. Sun, B. Chen, and X. Yuan, "Voltage sag forming method considering transient process," in *Proc. IEEE 4th Inf. Technol. Mechatronics Eng. Conf. (ITOEC)*, Dec. 2018, pp. 1204–1208.
[21] G. Olguin, "An optimal trade-off between monitoring and simulation for voltage dip characterization of transmission systems," in *Proc. IEEE/PES Transmiss. Distrib. Conf. Expo., Asia Pacific*, Aug. 2005, pp. 1–6.
[22] M. T. A. Begum, M. R. Alam, and K. M. Muttaqi, "Analytical expressions for characterising voltage dips and phase-angle jumps in electricity networks," *IET Gener., Transmiss. Distrib.*, vol. 13, no. 1, pp. 116–126, Jan. 2019.
[23] S. O. Faried and S. Aboreshaid, "Stochastic evaluation of voltage sags in series capacitor compensated radial distribution systems," *IEEE Trans. Power Del.*, vol. 18, no. 3, pp. 744–750, Jul. 2003.
[24] J. L. Blackburn, *Protective Relaying: Principles and Applications*. New York, NY, USA: Marcel Dekker, 1987.
[25] H. Orsila, E. Salminen, and T. Hämäläinen, "Recommendations for using simulated annealing in task mapping," *Design Autom. Embedded Syst.*, vol. 17, no. 1, pp. 53–85, Mar. 2013.
[26] F. Ferrandi, P. L. Lanzi, C. Pilato, D. Sciuto, and A. Tumeo, "Ant colony heuristic for mapping and scheduling tasks and communications on heterogeneous embedded systems," *IEEE Trans. Comput.-Aided Design Integr. Circuits Syst.*, vol. 29, no. 6, pp. 911–924, Jun. 2010.
[27] Y. Zhang, S. Wang, and G. Ji, "A comprehensive survey on particle swarm optimization algorithm and its applications," *Math. Problems Eng.*, vol. 2015, pp. 1–38, Oct. 2015.
[28] M. A. Hannan, M. G. M. Abdolrasol, M. Faisal, P. J. Ker, R. A. Begum, and A. Hussain, "Binary particle swarm optimization for scheduling MG integrated virtual power plant toward energy saving," *IEEE Access*, vol. 7, pp. 107937–107951, 2019.
[29] J. Kennedy and R. C. Eberhart, "A discrete binary version of the particle swarm algorithm," in *Proc. IEEE Int. Conf. Syst., Man, Cybern., Comput. Cybern. Simulation*, Oct. 1997, pp. 4104–4108.
[30] J. A. Martinez and J. Martin-Arnedo, "Voltage sag studies in distribution Networks—Part II: Voltage sag assessment," *IEEE Trans. Power Del.*, vol. 21, no. 3, pp. 1679–1688, Jul. 2006.
[31] J. A. Martinez and J. Martin-Arnedo, "Voltage sag studies in distribution Networks—Part III: Voltage sag index calculation," *IEEE Trans. Power Del.*, vol. 21, no. 3, pp. 1689–1697, Jul. 2006.
[32] J. Blanco-Solano, J. F. Petit-Suarez, G. Ordonez-Plata, and N. Kagan, "Voltage sag state estimation using compressive sensing in power systems," in *Proc. IEEE Milan PowerTech*, Milan, Italy, Jun. 2019, pp. 1–6.
[33] X. Zambrano, A. Hernandez, M. Izzeddine, and R. M. de Castro, "Estimation of voltage sags from a limited set of monitors in power systems," *IEEE Trans. Power Del.*, vol. 32, no. 2, pp. 656–665, Apr. 2017.
[34] A. D. Santos, T. Rosa, and M. T. Correia de Barros, "Stochastic characterization of voltage sag occurrence based on field data," *IEEE Trans. Power Del.*, vol. 34, no. 2, pp. 496–504, Apr. 2019.

HAIWEI JIANG was born in Jinzhou, Liaoning, China, in 1996. He received the B.S. degree in electrical engineering and automation from Dalian Jiaotong University. He is currently pursuing the M.S. degree with North China Electric Power University. His research interests include power quality and its control.

YONGHAI XU (Member, IEEE) was born in Henan, China, in 1966. He received the B.S. degree from Tsinghua University, Beijing, China, in 1989, the M.S. degree from North China Electric Power University, Beijing, in 1992, and the Ph.D. degree from the Harbin Institute of Technology, Harbin, China, in 2002, all in electrical engineering.

He is currently a Professor at the School of Electrical and Electronic Engineering, North China Electric Power University. His research interests include power quality analysis and control, power electronic transformer, and new energy power systems.

ZITENG LIU was born in Bozhou, Anhui, China, in 1996. She received the B.S. degree from China Agricultural University. She is currently pursuing the M.S. degree with North China Electric Power University. Her research interests include power quality and its control.

NING MA was born in Qingdao, Shandong, in 1996. He received the B.S. degree in electrical engineering and automation from the Shandong University of Technology. He is currently pursuing the M.S. degree with North China Electric Power University. His research interests include power quality analysis and control.

WENQING LU (Graduate Student Member, IEEE) was born in Fuzhou, Fujian, China, in 1994. She received the B.S. degree in smart grid information engineering from North China Electric Power University, where she is currently pursuing the M.S. degree. Her research interests include power quality and its control.